16TH EUROPEAN CONFERENCE ON EARTHQUAKE ENGINEERING THESSALONIKI 18 - 21 JUNE 2018

A LOOK AT THE SEISMIC RISK OF ITALIAN CODE-CONFORMING RC BUILDINGS

Akiko SUZUKI,[1] Georgios BALTZOPOULOS,[2] Iunio IERVOLINO,[3] and the RINTC WP4 Workgroup[4]

ABSTRACT

This paper discusses the seismic risk of some structures designed, modeled and analyzed within the RINTC (*Rischio Implicito di strutture progettate secondo le Norme Tecniche per le Costruzioni*) project. RINTC, funded by the *Italian Department for Civil Protection* is a multiple-year effort that started in 2015 as a joint collaboration between ReLUIS (*Rete dei Laboratori Universitari di Ingegneria Sismica*) and EUCENTRE (*Centro Europeo di Formazione e Ricerca in Ingegneria Sismica*). In the project, the structures, with a variety of structural types, configurations and locations, spanning a wide range of seismic hazard levels, were designed in compliance with the current Italian code provisions, while their seismic risk was computed, in terms of annual failure rate, following the framework of performance-based earthquake engineering. The results of RINTC, although not yet fully consolidated, show, among other features, a generally increasing trend of the annual collapse rates with the increasing hazard of the sites. This study, aiming at investigating the preliminary results of RINTC, examines structural response to gather insights on the homogeneity of the collapse risk among the prototype buildings. In particular, the reinforced concrete moment-resisting frames are examined using single-degree-of freedom systems equivalent to the detailed structural models, in order to capture the overall tendencies of their seismic behavior. It appears that the increasing trend of the failure rates with site hazard is reflected in the actual strength reduction factors of the equivalent systems, despite the uniform value of the behavior factor was set to define the reference design strength of the buildings.

Keywords: Performance-based earthquake engineering; failure rate; NTC08.

1. INTRODUCTION

In the current Italian building code (Consiglio Superiore Lavori Pubblici, 2008; NTC08 hereafter) similar to Eurocode 8 (CEN, 2004), structural performance with respect to violation of given limit states (*failure* hereafter), has to be verified for levels of ground motions associated with specific exceedance return periods, T_R, at the building site. In case of ordinary structures, for example, safety verifications for life-safety and collapse limit states are required against ground motion levels corresponding to T_R of 475 and 975 years (probabilities of exceedance of 10% and 5% in 50 years), respectively. In such design practice, thanks to code requirements, it is generally expected that the probability of failure will be smaller than that of exceedance of the design ground motion intensity; however, the safety margins at the structure level are not explicitly controlled during design.

To quantitatively address the seismic risk that the code-conforming design implicitly exposes structures to, a large research project is undergoing in Italy. This project, named *Rischio Implicito – Norme*

[1]Ph.D. candidate, Dipartimento di Strutture per l'Ingegneria e l'Architettura, Università degli Studi di Napoli Federico II, Naples, Italy, akiko.suzuki@unina.it

[2]Assistant professor, Dipartimento di Strutture per l'Ingegneria e l'Architettura, Università degli Studi di Napoli Federico II, Naples, Italy, georgios.baltzopoulos@unina.it

[3]Full professor, Dipartimento di Strutture per l'Ingegneria e l'Architettura, Università degli Studi di Napoli Federico II, Naples, Italy, iunio.iervolino@unina.it

[4]Paolo FRANCHIN (Univ. Sapienza di Roma), Gennaro MAGLIULO (Univ. di Napoli Federico II), Angelo MASI (Univ. della Basilicata), Fabrizio MOLLAIOLI (Univ. Sapienza di Roma), Enrico SPACONE (Univ. di Chieti-Pescara Gabriele D'Annunzio), Gerardo VERDERAME (Univ. di Napoli Federico II).

Tecniche per le Costruzioni (RINTC), has been developed by the joint working group between *Rete dei Laboratori Universitari di Ingegneria Sismica* (ReLUIS) and *Centro Europeo di Ricerca e Formazione in Ingegneria Sismica* (EUCENTRE), with the funding of *Dipartimento della Protezione Civile* (DPC) (http://www.reluis.it/index.php?option=com_content&view=article&id=549&Itemid=19__8&lang=it). In this project, structures belonging to a variety of structural types (i.e., un-reinforced masonry (URM), reinforced concrete (RC), precast reinforced concrete (PRC), steel, and base isolated reinforced concrete (BI) buildings) and configurations, were designed according to the current Italian code provisions in a number of sites at different hazard levels (Milan, Caltanissetta, Rome, Naples, and L'Aquila) and local site conditions (A and C according to Eurocode 8 classification; see RINTC workgroup, 2017).
Figure 1a,b shows the locations and hazard curves at the five sites on site class C, in terms of annual exceedance rate of peak ground acceleration (PGA), respectively. The hazard curves were computed considering the seismic source model described in Meletti et al. (2008) and the ground motion prediction equation of Ambraseys (1996) as described in Iervolino et al. (2017).

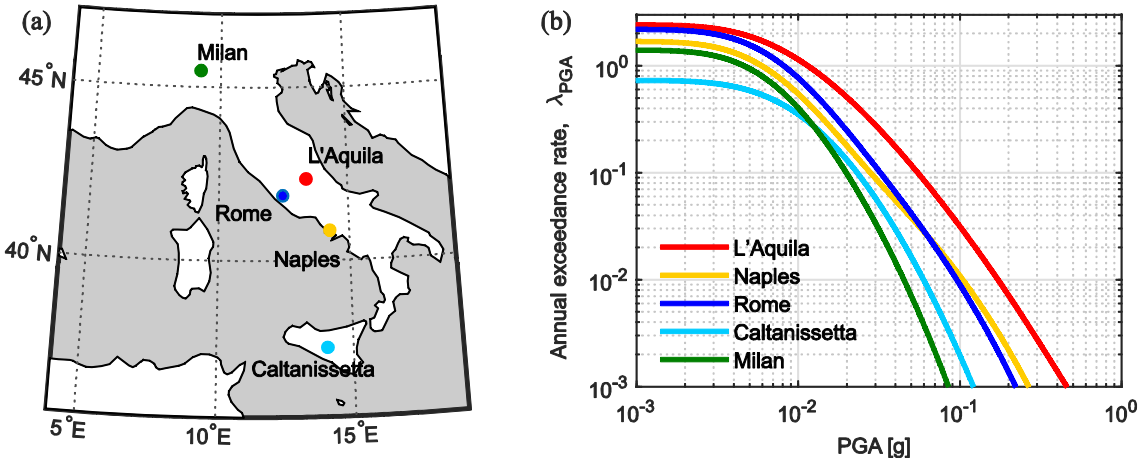

Figure 1. Selected five Italian cities; (a) locations; (b) annual exceedance rate of PGA on soil site class C according to Eurocode 8 classification.

The seismic risk of the designed structures (e.g., annual collapse and damage onset rates) is then quantified by a state-of-the-art approach referring to performance-based earthquake engineering, which includes multi-stripe dynamic analysis of the three-dimensional (3D) structural models and integration of probabilistic hazard with probabilistic vulnerability. The failure criteria are defined in a uniform manner among structures belonging to the same typology.
As a summary of the results of RINTC, Figure 2 reports the collapse failure rates (see the following sections for computation details) for the prototype buildings designed at three out of the five sites (i.e., Milan, Naples, and L'Aquila), those arranged in ascending order of design hazard at the site. Although the results of the RINTC project, which is a large research effort, cannot be yet considered fully consolidated, as verifications and adjustments are still ongoing, some general findings already deserve deeper scrutiny: (i) the heterogeneity of seismic safety among structural types designed for the same hazard and (ii) a general trend of increasing risk with the increasing design hazard of the building site (Iervolino et al. 2017). Some may argue that (i) is well expected due to the different design procedures which pertain to different structural types (e.g., RC and URM buildings); on the other hand, (ii) may be less expected.
The simple investigations discussed in this paper aim at starting to examine the trend depicted in Figure 2 with respect to seismic structural features that originate from design. In particular, those of RC buildings are examined out of the five structural types covered in the project. For this purpose, the structural models used in the RINTC project are converted into equivalent single-degree-of-freedom (ESDOF) systems via the static pushover (SPO) curves of the 3D structural models. The approximation introduced is verified through the comparison of the failure rates between the original and simplified models using the same risk calculation procedure as was used in the project. The ESDOF systems are used to derive basic comparative information, such as strength modification factors and failure ductility capacities, to compare among the structures.

The remainder of the paper is structured such that the next section describes the prototype buildings covered in this study, including their ESDOF characterization. Subsequently, the failure rates obtained for the ESDOF are compared with those from the original models. Then, some design structural features of those structures are presented to address the observed trend of seismic risk. Final remarks close the study.

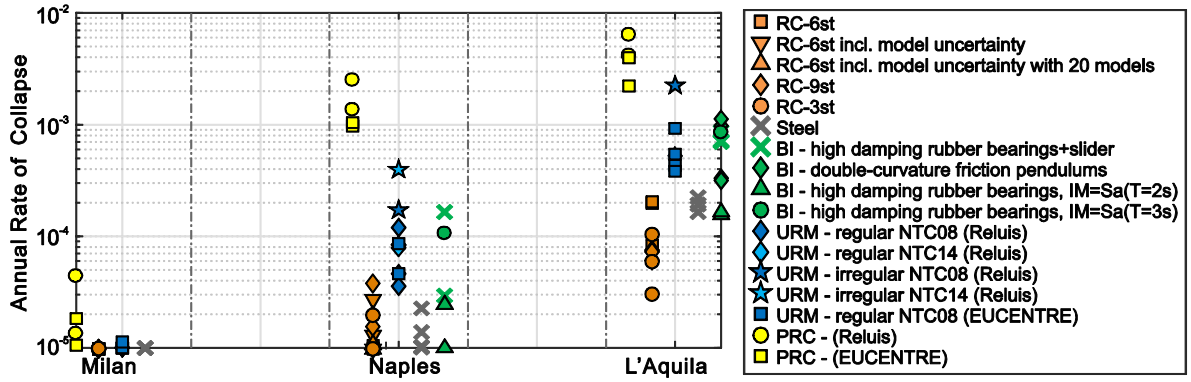

Figure 2. Annual collapse rates of the prototype buildings of the RINTC project (site class C); for the detailed classification of the considered buildings, see RINTC workgroup (2017) and Iervolino et al. (2017).

2. STRUCTURES AND NUMERICAL MODELS

2.1 Prototype RC buildings of the RINTC project

In the RINTC project, series of three-, six-, and nine-story RC moment-resisting frame buildings were designed according to the NTC08 design code for the *life-safety* limit state defined in the codes. In case of the six-story buildings, three different structural configurations (i.e., bare-, infilled-, and pilotis frames, hereafter denoted as BF, IF, and PF, respectively; Figure 3a) were considered for each of the five Italian sites (on site class C) with different levels of seismicity. For three of the five sites three- and nine-story buildings were also designed (Camata et al. 2017). These buildings, intended for residential use, were all 5x3-bay moment-resisting frames characterized by regularity in plan and elevation. The ground level was 3.4m high while all other stories were 3.05m high. The RC frames included knee-joint beams designed to bear the staircases. From a design point of view, the structural members of BF and IF were identical in dimensions and reinforcement detailing (i.e., the difference lies in the presence of infills) while the vertical structural members of PF were strengthened to account for the infill reduction at the ground floor, as per code requirements.
For each site, seismic design was performed by means of modal response spectrum analysis. The reference design strength was assigned by the design response spectrum that is obtained from the horizontal elastic response spectrum, which is actually an approximation of the 475 years return period uniform hazard spectrum (UHS) for the site, divided by the behavior factor q. It should be mentioned that the NTC08 prescribes q factor for a structure depending on typology, ductility level, and regularity of the structural system. For the prototype buildings of the project, the q factor was set to q = 3.9 (NTC08, § 7.4.3.2) for the bare frames at all sites (masonry infills are not explicitly accounted for during design to NTC08, hence the reference to BF alone covering all frames).
In order to perform structural response analyses, 3D numerical models of these prototype buildings were constructed in OpenSees software (McKenna et al. 2000). For more details on the structural design and subsequent numerical modelling, see Camata et al. (2017) and RINTC workgroup (2017).

2.2 ESDOF characterization of the prototype buildings

Among the prototype RC buildings described above, those designed for the three sites with a complete set of the three different number of stories and configurations, i.e., Milan, Naples, and L'Aquila, were exclusively considered in this study. In particular, the structural design features of the selected buildings

were examined through the ESDOF systems converted from the 3D structural models of the project. This approximation, based on the static capacity curves of the structures, facilitates to capture the overall trends of structural demands and capacities among a large number of different structures, in addition to reducing computational demands of the original detailed models. The conversion to an ESDOF model involves the definition of the SDOF oscillator's characteristics such as the equivalent mass m^* and vibration period T^* and SPO backbone parameters, which are defined based on the SPO curves and modal contribution of the dominant vibration mode of the original multi (n)-story structural models. Figure 4 illustrates the detailed conversion process of the 3D structural models of the prototype RC buildings. First of all, SPO analysis was carried out per principal direction of each 3D structural model using modal load distribution, in which the load profile F_i, the product of the floor mass m_i and the dimensionless displacement profile ϕ_i, was applied to each floor level, $i = \{1, 2, \ldots, n\}$ (Figure 4a). The obtained SPO curve was then multi-linearized to characterize force-displacement relationship of the original structure. Approximating the original frame model with a lumped mass multiple-degree-of-freedom (MDOF) system, the MDOF quantities were subsequently transformed to those of the ESDOF system (Fajfar 2000) as follows (Figure 4b): the equivalent mass was given by $m^* = \sum_{i=1}^{n} m_i \phi_i$, while the equivalent vibration period T^* was determined as $T^* = 2\pi\sqrt{m^* \delta_y^* / F_y^*}$, where F_y^* and δ_y^* were the yield strength and the yield displacement of the multi-linearized SPO curve, F_y and δ_y, respectively, divided by the modal participation factor, $\Gamma = m^* / \sum_{i=1}^{n} m_i \phi_i^2$; the yielding spectral acceleration at the equivalent period is then obtained by $Sa_y\left(T^*\right) = F_y^* / m^*$; the damping ratio of the ESDOF system ξ^* was set to be equivalent to the one at the dominant vibration mode of the original structural model (5% in this study). Meanwhile, the SPO backbone curve of the ESDOF system was derived from the multi-linear-fitted SPO curve scaled down by Γ, maintaining the same dimensionless parameters to characterize the multi-linear backbone, such as the capping-point ductility μ_c and failure ductility μ_f (Figure 4c). For the given SPO parameters, a moderately pinching, peak-oriented hysteretic behavior without any cyclic stiffness/strength deterioration (e.g., Vamvatsikos and Cornell 2005) was applied, assuming it can approximately represent the overall structural responses of generic RC buildings.

It should be noted that, in this study, the static capacities in two horizontal directions were examined independently, by defining two uncoupled ESDOF systems for each structure that represent the structural capacities in two horizontal directions (i.e., X and Y in Figure 4).

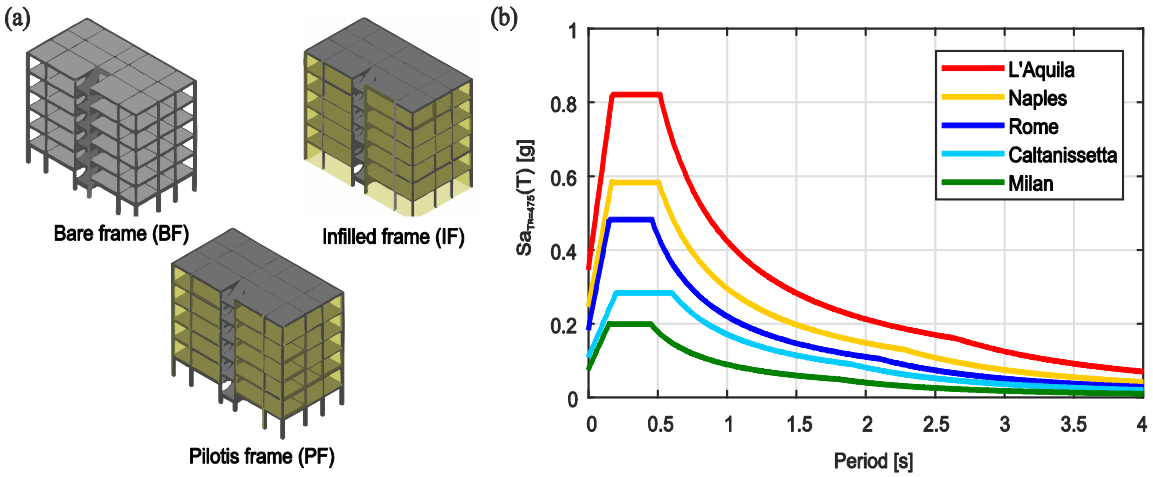

Figure 3. RC buildings; (a) three types of structural configurations; (b) horizontal elastic spectra at the five sites (site class C), which are approximations the UHS' with 475 years return period of exceedance at each site.

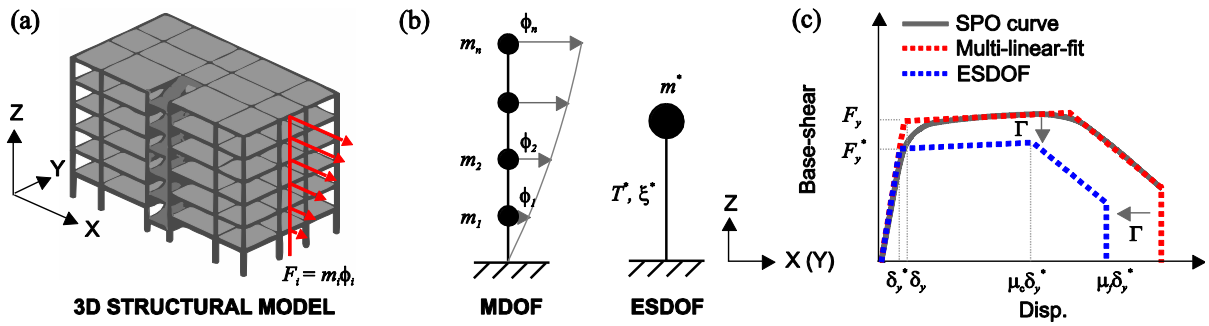

Figure 4. ESDOF conversion; (a) SPO analysis with 3D model; (b) ESDOF conversion through lumped mass MDOF approximation; (c) characterization of SPO backbone of the ESDOF system.

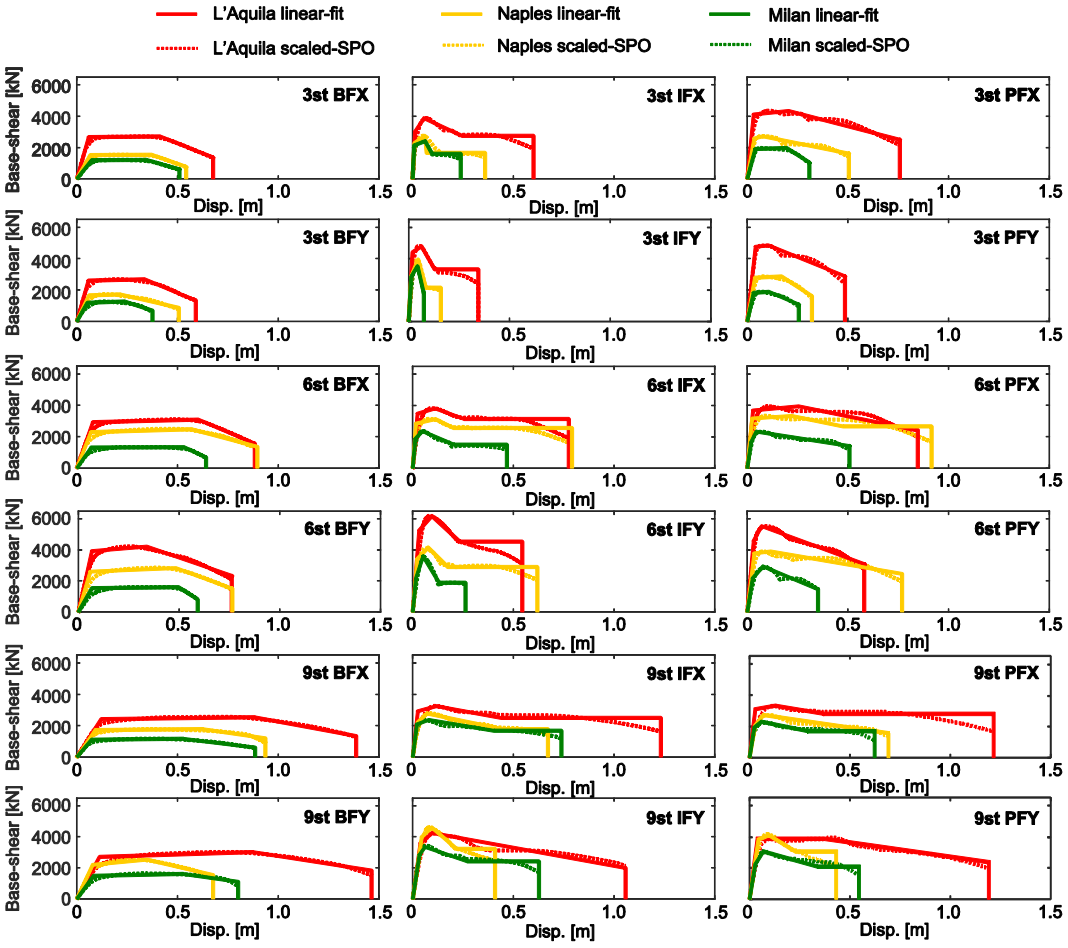

Figure 5. ESDOF-SPO backbones of the prototype RC buildings.

Figure 5 shows the SPO backbones of the obtained ESDOF systems of the prototype buildings, with the three different number of stories, configurations at the three sites, for two horizontal (i.e., X and Y) directions. In each panel of the figures, the piecewise-linear-fitted SPO backbones of the ESDOF systems are compared with the scaled ones of the MDOF systems. It should be mentioned that the collapse criterion for the original 3D frame models was defined based on the roof displacement at which base-shear on the SPO curve drops to 50% of the maximum resistance. For the structures with the same number of stories, their static load capacity reflects the design hazard of the site (i.e., in order of Milan, Naples, and L'Aquila) while IF and PF have higher strength and stiffness than BF due to the additional lateral strength provided by the infill walls. Through the tri-linear or quadri-linear idealization of each SPO backbone (Baltzopoulos et al. 2017), the structural parameters of the ESDOF systems were determined for all the considered buildings. These parameters are summarized in Tables 1a-c, for the

three-, six- and nine-story buildings, respectively. It should also be noted that the first vibration periods in the direction of interest, T_1, were derived from the eigenvalue analysis of the original 3D frames and do not necessarily coincide with the equivalent period, T^*. Nonetheless, the computed ESDOF systems exhibited some consistency with the original structures, which will be further verified in terms of failure rate estimation in the next section.

Table 1a. Structural parameters of three-story RC buildings at the three sites.

Config. /Site	Dir.	F_y [kN]	T_1 [s]	T^* [s]	m^* [ton]	F_y^* [kN]	$Sa_y(T^*)$ [g]	$Sa_{T_R=475}(T^*)$ [g]	$T_{R,Say(T^*)}$ [years]
BF Milan	**X**	1542	1.04	1.10	497	1201	0.25	0.08	$>10^5$
	Y	1492	0.90	0.95	508	1171	0.23	0.09	38820
BF Naples	**X**	1959	0.89	0.93	496	1520	0.31	0.32	1313
	Y	2100	0.83	0.86	510	1643	0.33	0.34	1058
BF L'Aquila	**X**	3455	0.66	0.68	534	2668	0.51	0.62	431
	Y	3344	0.67	0.69	543	2600	0.49	0.61	401
IF Milan	**X**	2718	0.21	0.27	517	2154	0.43	0.20	13319
	Y	3584	0.24	0.30	524	2851	0.55	0.20	36887
IF Naples	**X**	2898	0.22	0.28	531	2302	0.44	0.58	346
	Y	3642	0.24	0.31	538	2907	0.55	0.58	589
IF L'Aquila	**X**	3839	0.23	0.30	580	3059	0.54	0.82	179
	Y	5514	0.25	0.33	590	4422	0.76	0.82	379
PF Milan	**X**	1956	0.74	0.76	701	1905	0.28	0.12	31686
	Y	1891	0.67	0.69	693	1821	0.27	0.13	14039
PF Naples	**X**	2709	0.60	0.62	703	2594	0.38	0.48	553
	Y	2912	0.60	0.62	700	2776	0.40	0.48	663
PF L'Aquila	**X**	4506	0.43	0.47	730	4119	0.58	0.82	309
	Y	5198	0.50	0.50	731	4754	0.66	0.82	414

Table 1b. Structural parameters of six-story RC buildings at the three sites.

Config. /Site	Dir.	F_y [kN]	T_1 [s]	T^* [s]	m^* [ton]	F_y^* [kN]	$Sa_y(T^*)$ [g]	$Sa_{T_R=475}(T^*)$ [g]	$T_{R,Say(T^*)}$ [years]
BF Milan	**X**	1658	1.70	1.70	1245	1299	0.11	0.05	34495
	Y	1924	1.48	1.48	1283	1529	0.12	0.06	34771
BF Naples	**X**	2935	1.25	1.25	1306	2283	0.18	0.24	799
	Y	3300	1.11	1.11	1376	2618	0.19	0.27	632
BF L'Aquila	**X**	3829	1.13	1.13	1177	2923	0.25	0.38	380
	Y	5246	0.88	0.87	1147	3941	0.35	0.49	345
IF Milan	**X**	2458	0.53	0.53	1161	1865	0.16	0.17	1235
	Y	2874	0.58	0.58	1165	2164	0.19	0.15	2319
IF Naples	**X**	3714	0.52	0.53	1265	2842	0.23	0.56	158
	Y	4493	0.57	0.57	1262	3419	0.28	0.52	234
IF L'Aquila	**X**	4544	0.51	0.57	1230	3485	0.29	0.74	115
	Y	6827	0.50	0.54	1247	5269	0.43	0.78	227
PF Milan	**X**	1874	0.92	0.92	1616	1636	0.10	0.10	1824
	Y	2597	0.88	0.88	1533	2184	0.15	0.10	5565
PF Naples	**X**	3874	0.69	0.69	1560	3170	0.21	0.43	201
	Y	4672	0.73	0.73	1530	3787	0.25	0.40	411
PF L'Aquila	**X**	4616	0.60	0.65	1401	3671	0.27	0.65	134
	Y	6080	0.54	0.57	1251	4581	0.37	0.74	178

Table 1c. Structural parameters of nine-story RC buildings at the three sites.

Config. /Site	Dir.	F_y [kN]	T_1 [s]	T^* [s]	m^* [ton]	F_y^* [kN]	$Sa_y(T^*)$ [g]	$Sa_{T_R=475}(T^*)$ [g]	$T_{R,Say(T^*)}$ [years]
BF Milan	**X**	1451	2.12	2.09	1684	1105	0.07	0.04	10627
	Y	1944	1.93	1.93	1677	1472	0.09	0.04	22578
BF Naples	**X**	2262	1.88	1.92	1763	1711	0.10	0.15	725
	Y	2972	1.55	1.56	1721	2208	0.13	0.19	829
BF L'Aquila	**X**	3181	1.86	1.86	1774	2423	0.14	0.23	553
	Y	3639	1.67	1.68	1725	2707	0.16	0.25	516
IF Milan	**X**	2811	0.77	0.77	1639	2094	0.13	0.12	2169
	Y	3892	0.84	0.84	1591	2846	0.18	0.11	9434
IF Naples	**X**	2941	0.89	0.90	1829	2228	0.12	0.33	136
	Y	5329	0.88	0.89	1792	3983	0.23	0.33	488
IF L'Aquila	**X**	3844	0.76	0.78	1728	2936	0.17	0.54	104
	Y	4874	0.84	0.84	1695	3589	0.22	0.50	162
PF Milan	**X**	2423	0.97	0.97	2011	1898	0.10	0.09	1666
	Y	2945	1.00	1.00	1886	2232	0.12	0.09	4143
PF Naples	**X**	2723	0.99	1.00	2012	2106	0.11	0.30	93
	Y	5082	0.94	0.95	1917	3847	0.21	0.31	302
PF L'Aquila	**X**	4077	0.89	0.87	2012	3140	0.16	0.49	100
	Y	5148	0.89	0.89	1853	3859	0.21	0.48	177

3. COLLAPSE RISK

3.1 RINTC risk assessment scheme

In the RINTC project the seismic risk of a structure is quantified as the expected number in one year of earthquakes capable to fail the structure at the site; i.e., *failure rate,* λ_f. This is obtained via Equation (1), that is by integrating a probabilistic representation of structural fragility, $P\left[\, failure \middle| IM = im \right]$, and probabilistic seismic hazard. Hazard is represented by means of the annual rate of exceedance, λ_{im}, of the values (*im*) of a ground motion intensity measure (*IM*) computed through probabilistic seismic hazard analysis (PSHA; Cornell and Krawinkler 2000).

$$\lambda_f = \int_{im} P\left[\, failure \,|\, IM = im \right] \left| d\lambda_{im} \right| \tag{1}$$

In the RINTC project, the term $P\left[\, failure \middle| IM = im \right]$ was computed through *multiple stripe analysis* (MSA, e.g., Jalayer and Cornell 2003) of the 3D nonlinear structural models, at ten *IM* levels corresponding to return periods from 10 up to 10^5 years, at each site. In the following, these *IMs* will also be indicated as *IML*.

Record selection was hazard-consistent by means of the *conditional spectrum* approach (e.g., Lin et al. 2013; see Iervolino et al. 2017 for details). The ground motion *IM* was selected depending on the number of stories and structural configurations of the buildings: in the case of six-story RC buildings, $Sa(1.5s)$ and $Sa(0.5s)$ were defined as *IM*s for BF and for IF/PF frames, respectively, due to the proximity of their first mode vibration periods. Structural *failure* was considered to have been reached in cases of global instability (according to Shome and Cornell 2000) or whenever measured maximum ductility response exceeded the failure ductility, μ_f, in either horizontal direction.

It should be noted that, in order to avoid large extrapolations, PSHA for each site was carried out only up to the *im*-value with 10^5 years exceedance return period, say im^*. For this reason, the computed

failure rates assume that $P\left[\, failure \,|\, IM = im \,\right] = 1, \forall im > im^*$. Equation (2) gives the expression for λ_f^*, from which it appears that this is necessarily a conservative approximation of the *true* rate, λ_f.

$$\lambda_f^* = \int_0^{im^*} P\left[\, failure \,|\, IM = im_i \,\right] \cdot \left| d\lambda_{im} \right| + \lambda_{im^*} = \int_0^{im^*} P\left[\, failure \,|\, IM = im_i \,\right] \cdot \left| d\lambda_{im} \right| + 10^{-5} \tag{2}$$

3.2 ESDOF failure rates

In order to evaluate the accuracy of the ESDOF approximation employed in Section 2.2, the failure rates of the ESDOF systems were estimated in a manner similar to that described in the previous section for the original structural models. It should be mentioned that this study examined structural responses of two horizontal structural planes individually, while the coupled responses were accounted for in the project through the simultaneous input of pairs of horizontal accelerograms to the 3D models. Hence, for every structure, the ESDOF system of each horizontal direction was shaken by either of two horizontal components of a ground motion record, then all cases where the measured maximum ductility response exceeded the failure ductility, μ_f, in either of the two horizontal directions were treated as structural *failure*, same as for the original structures.

Figure 6 shows the failure rates computed for the ESDOF systems compared to those for the MDOF systems. In each figure, the rates for the three different configurations are plotted for the sites, aligned in ascending order of the design hazard. It is observed that the failure rates computed using ESDOF models are in general agreement with the ones for the original models, showing the same trend of increasing risk with increasing hazard. In most cases, the computed failure rates for two different systems for each structure have the same orders of magnitude, ranging from 10^{-5} to 10^{-4}. Since Equation 2 provides an approximate value of the *true* failure rate λ_f, the rates excluding the contribution from *IM*s larger than im^*, $\lambda_f^* - \lambda_{im^*}$, are also shown in Figure 7.

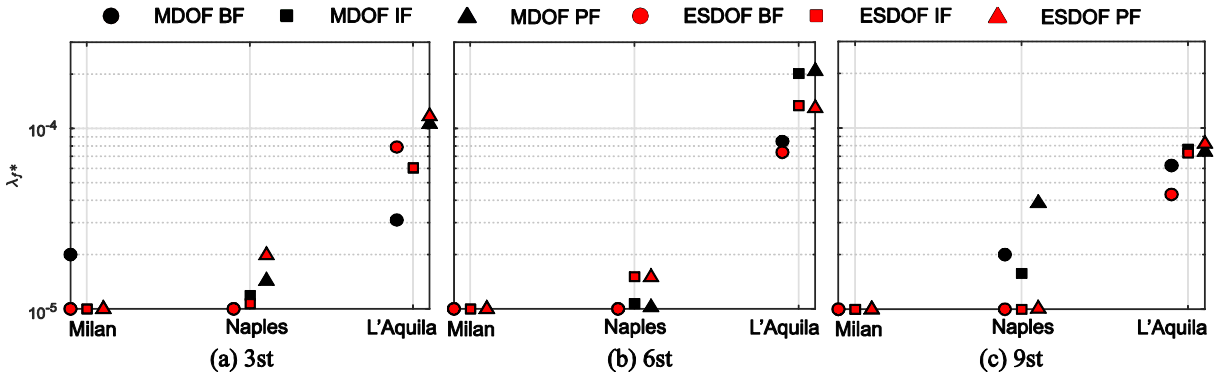

Figure 6. Failure rates for the prototype RC buildings (estimated via Equation 2).

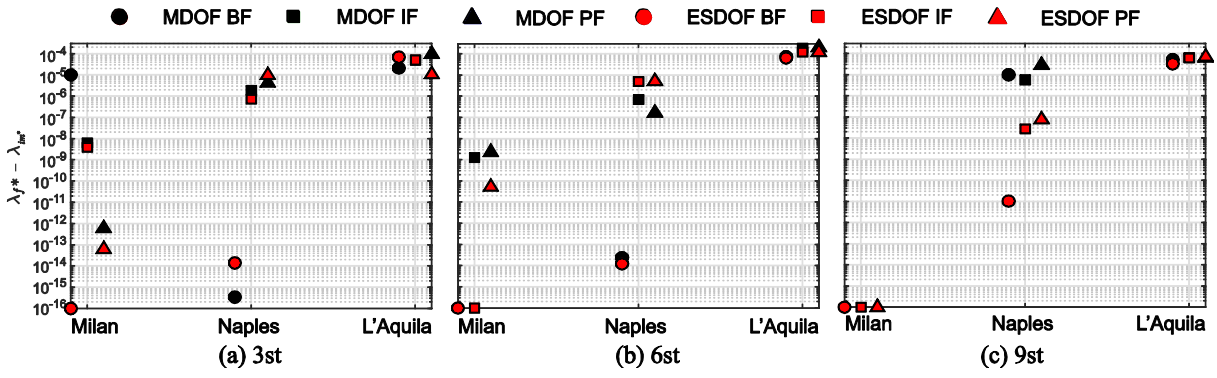

Figure 7. Failure rates for the prototype RC buildings (subtracting the maximum error of 10^{-5} from Equation 2).

It is shown, through this comparison, that the ESDOF-based failure rates can capture the rates for MDOFs even in the cases where the rates are smaller than λ_{im^*}, for which the trend is not visible due to the conservative approximation already discussed. For some cases, however, the orders of magnitude of the computed failure rates show some discrepancies between MDOF and ESDOF models, this is the case where more collapse cases occurred due to the numerical instability in the dynamic analyses with MDOF models while those were not observed with ESDOF models (e.g., Milan 3-story BF, Naples 9-story). Nonetheless, it can be considered that the pushover-based ESDOF models developed in this study represent well the overall features of seismic risk for the detailed structural models of the project.
It is also noteworthy that the trends across all three sites and configurations appear to be emphasized through the consideration on $\lambda_f^* - \lambda_{im^*}$. The failure rates at Naples and Milan are found to be much smaller not only than those at L'Aquila but also than the approximated rates shown in Figure 6, thus the rates λ_f^* are governed by the term λ_{im^*} employed in Equation 2. Regarding the different configurations, the failure rates of IF and PF are generally larger than those of BF while a less obvious trend is observed among buildings with different number of stories.

4. DESIGN TRENDS OF STRUCTURAL FEATURES

This section examines certain structural features of the prototype buildings resulting from code-conforming design, that can help explain the observed trend of seismic risk. In particular, emphasis is herein placed on the (global) strength and ductility characteristics, which are critical in determining the seismic capacity of structures. As briefly described above, the NTC08 standard prescribes the design lateral strength accounting for the hysteretic energy dissipation of the structure by means of the behavior factor, *q*, same as Eurocode 8 and other codes that espouse performance-based seismic design principles. The behavior factor *q* is used to reduce the elastic strength demand, with the tradeoff of acquiescing to plastic deformation under the design actions, and is thus prescribed by the code depending on structural typology, configuration and ductility class (NTC08, § 7.4.3.2). As mentioned, *q* was maintained constant for all structures at every site considered.
To better understand the trend of observed seismic risk with hazard, the strength reduction factors[5], $R_{T_R=475}$, for ESDOFs were computed herein. They are defined as the ratios of the horizontal acceleration at the equivalent oscillation period from the 475 year-return-period elastic design spectrum, $Sa_{T_R=475}\left(T^*\right)$, (Figure 3b) to the yield spectral acceleration of the ESDOF, $Sa_y\left(T^*\right)$: $R_{T_R=475} = Sa_{T_R=475}\left(T^*\right) / Sa_y\left(T^*\right)$. Figure 8a-c first compares the strength reduction factor $R_{T_R=475}$ across buildings with the three different heights (number of stories), sites, and structural configurations. In each panel corresponding to each building height, the three sites are aligned in the horizontal axis in order of seismicity level. It is observed that the strength reduction factor $R_{T_R=475}$ ranges from 0.3 to 3.7 depending on the case at hand, and that it tends to increase with increasing hazard level at the site, when compared between structures belonging to the same structural configuration and building height. In fact, the $R_{T_R=475}$ factors computed among the buildings at L'Aquila, the site with the severest hazard, were approximately up to four times as large as the strength reduction factors of the buildings at Milan, the site with the mildest hazard. These results show that the structures at the sites with low seismicity, tend to exhibit lower reduction factors because of greater overstrength. This was to be expected, since at lower-hazard sites the strength reserves of a structure are more heavily dependent on the minimum requirements of the code's design provisions. (At the time of writing, similar tendencies were also observed for some groups of the masonry buildings designed in the project). An alternative way of

[5] In many US seismic design documents (e.g., ASCE/SEI 7-05, FEMA P695) the letter "R" is used to denote the so-called *Response Modification Coefficient*, which is equivalent to the behavior factor *q* of NTC08 and EC8; the reader is thus cautioned against mistaking its use herein, which is to denote the strength reduction factor as defined at the ESDOF system level in the text.

highlighting this same effect, i.e., the fact that the structures designed for lower-hazard sites appear stronger than their higher-hazard counterparts, when lateral resistance is seen as a proportion of code-mandated elastic demand, is to monitor the return period of exceedance of the spectral acceleration causing nominal yield, $T_{R,Say(T^*)}$. This is provided in Tables 1a-c for the cases examined here; it can be observed that among counterpart structures, despite the increase of ESDOF yield force with increasing hazard, structures at higher-hazard levels are expected to experience excursions beyond their nominal yield point more frequently.

Meanwhile, Figure 8d-f compares failure ductility, which was computed for the ESDOFs, from the piece-wise linear SPO parameters in Section 2.2 (see Figure 5). Contrary to the clear trend exhibited by $R_{T_R=475}$, which is also reflected by a similar trend on yield frequency, no obvious trend was observed for μ_f across the structures at different sites nor across those with the same building height.

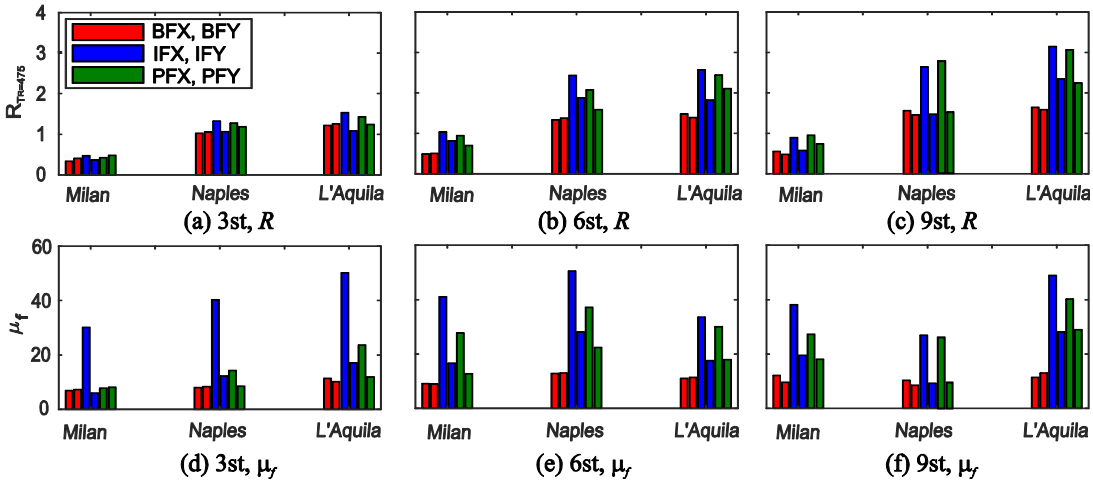

Figure 8. Comparison of inelastic capacity of the structures; (a-c) strength reduction factor; (d-f) failure ductility.

From these observations, it seems that the trend of $R_{T_R=475}$ is related to the observed trend of collapse risk. In fact, the differences of strength reduction factors between sites with different hazard levels, become much larger when the intensity measure levels corresponding to longer return periods are considered. Figure 9 shows the ratios of the exceedance level of spectral acceleration at the equivalent period for a given return period, which corresponds to each *IML* considered in Section 3.1, to the yielding strength for each structure, i.e., the strength reduction factor for a given return period, R_{T_R}.

It is observed that the R_{T_R} factor increases not only with the increase of return period, but also with the increase of hazard level at the site. Hence, the differences of R_{T_R} values between the three sites escalate with increasing return periods. At the maximum *IML* corresponding to 10^5 years exceedance return period, the R_{T_R} values for the L'Aquila buildings were found to be approximately up to twelve times as large as those for the Milan buildings. Moreover, the IF and PF buildings exhibit a significant increase of R_{T_R} at large *IM* levels due to the increase of hazard for short period structures.

At this point of investigation, it is indicated that the trend of strength reduction factor is one of the determining factors leading to the observed trend of seismic risk, since the non-linear ductility demand imposed by the earthquake is expected to scale with reduction factor. This fact needs to be further verified through similar investigation of the other structural typologies considered in the project. Moreover, there are other potentially contributing risk factors to be further examined during future work of the project, such as fragility and hazard modeling, as risk is a multiple variable function of a large number of structural and hazard parameters.

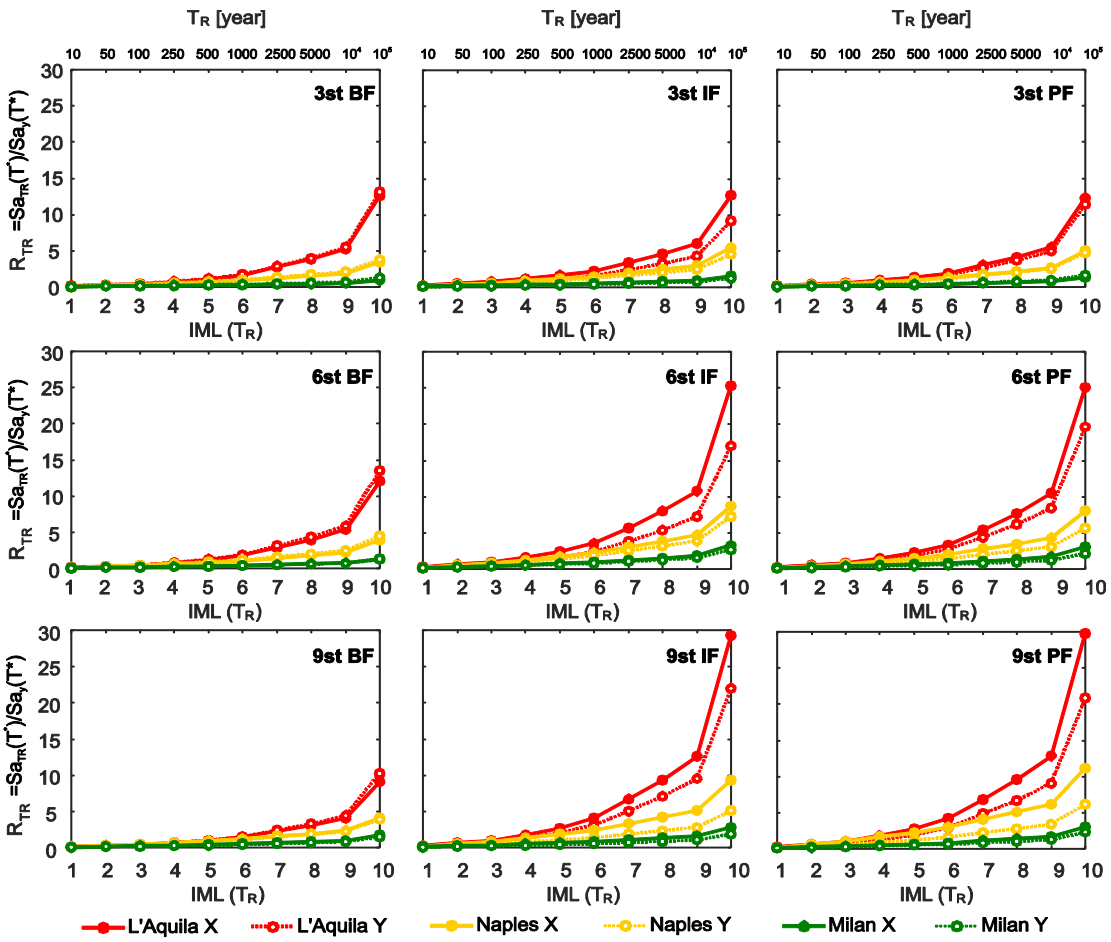

Figure 9. Strength reduction factor at each intensity measure level.

5. CONCLUSIONS

This short study examined structural features to explain the inhomogeneity of the collapse risk among the prototype buildings of the RINTC project. For the purposes of this investigation, the structural models used in the RINTC project were converted into ESDOF systems based on the static pushover (SPO) curves of the 3D structural models. Through this approximation, design trends of inelastic capacities such as strength reduction factors and ductility capacity up to failure were examined. The results of the study are:

1. the failure rates computed using ESDOF models have a degree of consistency with the ones for the original 3D structural models, showing the same trend of increasing risk as increasing hazard level at the site; in most cases, the computed failure rates for two different systems to represent each structure resulted in the same orders of magnitude, ranging from 10^{-5} to 10^{-4}, in case that a conservative approximation for earthquakes with the exceedance return period larger than 10^5 years was applied;
2. the strength reduction factors for the ESDOFs, tend to increase with an increase of the hazard at the site; conversely, the computed ductility capacity shows a less clear trend with respect to site hazard;
3. the study also showed that the reduction factor for a given return period R_{T_R} increased not only with the increasing return period, but also with the increasing hazard level at the site; this possibly means comparatively larger structural responses or more collapse cases, even at the seismic intensity level with the same exceedance probability, for the buildings designed at the site with higher seismicity.

As expected from a multivariable function of seismic risk, there are other risk contributing factors potentially as significant as the actual design strength. For this issue, a further examination on the

influences of the other risk contributing factors and those of the analytical approaches is underway. It should also be mentioned that the project is still ongoing, thus the findings presented above have to be verified through further investigation on other prototype buildings.

ACKNOWLEDGMENTS

The study was developed between 2015 and 2017 in the framework the *Rete dei Laboratori Universitari di Ingegneria Sismica* activities funded by *Presidenza del Consiglio dei Ministri – Dipartimento della Protezione Civile* (2014-2018 program).

REFERENCES

Ambraseys NN, Simpson KU, Bommer JJ (1996). Prediction of horizontal response spectra in Europe. *Earthquake Engineering & Structural Dynamics*, 25(4): 371-400.

Baltzopoulos G, Baraschino R, Iervolino I, Vamvatsikos D (2017). SPO2FRAG: Software for seismic fragility assessment based on static pushover. *Bulletin of Earthquake Engineering*, 15:4399–4425.

Camata G, Celano F, De Risi MT, Franchin P, Magliulo G, Manfredi V, Masi A, Mollaioli F, Noto F, Ricci P, Spacone E, Terrenzi M, Verderame G (2017). RINTC project: Nonlinear Dynamic Analyses of Italian code-conforming Reinforced Concrete Buildings for Risk of Collapse Assessment. *COMPDYN 2017 - 6th ECCOMAS Thematic Conference on Computational Methods in Structural Dynamics and Earth-quake Engineering*, M. Papadrakakis, M. Fragiadakis (eds.) Rhodes Island, Greece, 15–17 June.

CEN, European Committee for Standardization (2004). *Eurocode 8: Design Provisions for Earthquake Resistance of Structures, Part 1.1: General rules, seismic actions and rules for buildings, EN1998-1*.

Consiglio Superiore Lavori Pubblici, Decreto Ministeriale 14 gennaio (2008). Norme tecniche per le costruzioni (in Italian). *Gazzetta Ufficiale della Repubblica Italiana*, 29.

Cornell CA, Krawinkler H (2000). Progress and challenges in seismic performance assessment. *PEER Center News*, 3: 1-3.

Fajfar PA (2000). Nonlinear analysis method for performance-based seismic design. *Earthquake spectra*, 16(3): 573-592.

Iervolino I, Spillatura A, Bazzurro P (2017). RINTC project: Assessing the (implicit) seimsic risk of code-conforming structures in Italy. *Proc. of VI ECCOMAS Thematic Conference on Computational Methods in Structural Dynamics and Earthquake Engineering*, Rhodes, Greece, 15– 17 June.

Jalayer F, Cornell CA (2003). A technical framework for probability-based demand and capacity factor design (DCFD) seismic formats. PEER Report 2003/08, Pacific Earthquake Engineering Center, University of California,

Lin TG, Haselton CB, Baker JW (2013). Conditional spectrum‐based ground motion selection. Part I: Hazard consistency for risk‐based assessments. *Earthq Eng Struct D* 42:1847-1865.

Meletti C, Galadini F, Valensise G, Stucchi M, Basili R, Barba S, Vannucci G, Boschi E (2008). A seismic source zone model for the seismic hazard assessment of the Italian territory. *Tectonophysics*, 450(1): 85-108.

McKenna F, Fenves GL, Scott MH, Jeremic B (2000). Open System for Earthquake Engineering Simulation (OpenSees). Pacific Earthquake Engineering Research Center, University of California, Berkeley, CA.

RINTC Workgroup (2017). *Results of the 2015-2016 RINTC project*. ReLUIS report, ReLUIS, Naples, Italy.

Stucchi M, Meletti C, Montaldo V, Crowley H, Calvi GM, Boschi E (2011). Seismic hazard assessment (2003–2009) for the Italian building code. *B. Seismol. Soc. Am.*, 101: 1885- 1911.

Shome N, Cornell CA (2000). Structural seismic demand analysis: Consideration of "Collapse". In *PMC2000 - 8th ASCE Specialty Conference on Probabilistic Mechanics and Structural Reliability*. University of Notre Dame, South Bend, Indiana, 24-26 July 2000.

Vamvatsikos D, Cornell CA (2005). Direct estimation of seismic demand and capacity of multiple-degree-of-freedom systems through incremental dynamic analysis of single degree of freedom approximation. *J. Struct. Eng.*, 131:589–599.